How Does Vibrational Energy Flow Fill the Molecular State Space?

V. Wong and M. Gruebele*

Department of Chemistry and Beckman Institute for Advanced Science and Technology, University of Illinois at Urbana-Champaign, Urbana, Illinois 61801

Received: June 11, 1999; In Final Form: August 17, 1999

The experimental and theoretical evidence suggests that vibrational wave functions at high energy or in large molecules are not mixed to the maximum extent possible. One consequence is that average vibrational survival probabilities slow to a power law decay $t^{-\delta/2}$ with a small value of δ. An approximate formula is presented for estimating δ from the vibrational Hamiltonian and tested by comparing with wave packet propagations on an experimentally fitted potential surface of $SCCl_2$ in six degrees of freedom. Characterization of the wave packet by a dispersion parameter D furthermore shows that the state space accessed during vibrational energy flow remains nearly as compact as allowed by the decay law, opening the possibility for coherent control on a low-dimensional manifold embedded in the full vibrational state space.

1. Introduction

Vibrational spectra show features (groups of vibrational eigenstates with correlated intensities) even at high energy (E) or high density of states (ρ_{tot}).[1−4] Although the vibrational eigenfunctions may rapidly increase in complexity as E and ρ_{tot} increase, the wave functions associated with these features can remain quite simple. In small molecules, the origin of these features in the resonance structure of the Hamiltonian has been studied in terms of conserved polyad quantum numbers.[1,5]

Spectral features result from the interplay of the transition dipole operator, which weights the full density of eigenstates according to oscillator strength with the hierarchical structure of the vibrational Hamiltonian, which distributes the oscillator strength in a nontrivial fashion.[6] The hierarchical structure has several origins: the size of the potential constants and matrix elements decreases exponentially with the order of the coupling when dimensionless normal or local mode coordinates are used;[7−10] a "triangle rule" for vibrational matrix elements due to this exponential scaling restricts energy flow among triplets of states;[11] the local nature of most chemical bonding in large, low symmetry molecules reduces coupling among pairs and higher n-tuplets of vibrational states further.[12,13]

In larger molecules, a consequence of this hierarchy which has recently come to light is the slowness of vibrational dephasing (IVR) at intermediate times.[10,14] After a feature is prepared, a power law connects the short time quasi-exponential region of its survival probability to the long time region where a maximally diluted survival probability is obtained:

$$P(t) \sim t^{-\delta/2} \tag{1}$$

This was first suggested on the basis of a scaling analysis of diffusion or "hopping" of the vibrational wave packet density in state space.[14,15] δ could lie between 1 and $N-1$ or N, where the dimension N of the state space is the number of vibrational modes, and $\delta = N-1$ applies in the quasi-microcanonical limit usually realized in laser spectroscopy experiments. It should be noted that eq 1, like exponential dephasing, is a zero-order model. It arises as a result of a hierarchical structure of the Hamiltonian,[6] and could also be expressed as a correlated sum of exponential processes.[16] Unlike single exponential dynamics, eq 1 at least approximately builds these correlations right into the zero-order model.

A missing ingredient is a relationship between δ and the vibrational Hamiltonian. In particular, one would like to know how δ behaves for backbone vibrations (as opposed to XH vibrations), which are most important in chemical reactivity. It appears from experiments and simulations that δ rarely approaches N or $N-1$.[6,17] If IVR is indeed a quantum diffusion process in state space, it is confined to much lower dimension than the maximum possible. Here we present a simple formula for the dimensionality D_v of the state space manifold within which the IVR wave packet moves. D_v is obtained from the vibrational Hamiltonian without any dynamical calculation, by applying perturbation theory directly in the state space framework, as opposed to the usual time dependent perturbation theory leading to Fermi's Golden Rule. We compare D_v to numerical simulations of δ based on the high-quality experimentally fitted vibrational Hamiltonian of $SCCl_2$ with six degrees of freedom.[3] We obtain good agreement within the range of applicability of the formula. The dispersion of the vibrational wave packet is also studied in detail numerically and found to proceed through nearly the minimal number of vibrational features permitted by the observed power law decays. We introduce the dispersion D as a minimal parameter to describe the properties of the IVR wave function both at short times and at infinite time (i.e., the fully "relaxed" high-resolution spectrum of the vibrational eigenstates). These findings have important implications for the possibility of guiding molecular dephasing with coherent optical fields.[6]

2. Vibrational Dephasing Manifold

a. State Space. Figure 1 illustrates a vibrational state space in three dimensions.[10,14,18,19] Classically, the state space quantum numbers are directly related to action coordinates,[18] and the state space therefore has the same dimensionality as the vibrational coordinate space. Laser excitation is usually quasi-microcanonical. In a long time average, most states participating in the

* To whom correspondence should be addressed.

10.1021/jp9919361 CCC: $18.00 © 1999 American Chemical Society
Published on Web 09/23/1999

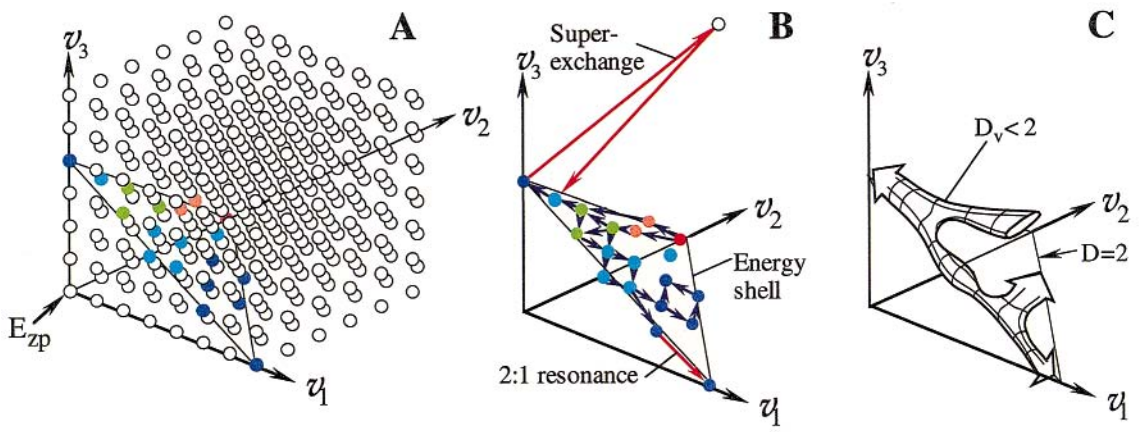

Figure 1. (A) Molecular state space in three dimensions. Each circle corresponds to a feature state with quantum numbers $\mathbf{n} = (v_1, v_2, ...)$. An energy shell and feature states near it are highlighted. (B) Energy shell and states from (A). The possibility of a superexchange chain is indicated by red arrows to a state off of the energy shell. A 2:1 resonance leading to IVR is also shown. The bright state $|0\rangle$ is shown in red, and successively accessible states are shaded across the spectrum to blue. The resonance structure of state space does not allow random flow among all feature states. (C) IVR flow manifold due to the resonances in (B). Because of energy conservation, its dimension must be ≤ 2 in the example shown. The actual dimension D_v lies somewhere between 1 and 2.

dynamics are therefore confined to an energy shell $E^{(0)} \pm \delta E$, where $E^{(0)}$ is the energy of the feature state which carries the oscillator strength (in red).

The states in Figure 1 are not vibrational eigenstates. Rather, they belong to a feature basis,[6,20] for example a normal or local mode basis, or one of the more exotic examples which have been studied in small systems.[21] Feature bases are characterized by a simple nodal structure and a complete set of well-defined quantum numbers **n**.

Feature bases include the "bright" states which carry the oscillator strength in spectroscopy experiments because of the Franck−Condon principle. For example, the initial state prepared at $t = 0$ of an ultrafast experiment usually has a simple, assignable structure. Likewise, in a high-resolution scan, there are spectral features which can be assigned, even though they may be fragmented into a set of perhaps unassignable eigenstates as in the insert to Figure 2.[3] Initiating IVR dynamics in a feature state therefore leads to a different class of dynamics than initiating dynamics in a highly dephased state which already resembles an eigenstate.[6]

In the state space of Figure 1, the "dark" states are also represented as feature basis states with well-defined quantum numbers **n**. All states are treated on an equal footing. This is very important and differs from the Golden Rule picture, whose bath states resemble eigenstates of the vibrational Hamiltonian (see section 3b). Unlike features, vibrational eigenstates have complex and perhaps unassignable nodal structures at sufficiently high E and ρ_{tot}.

If the full vibrational Hamiltonian is used for calculations, the exact choice of feature basis is irrelevant. Although the choice of initial feature state can affect the precise values of parameters such as δ in eq 1, it will be seen not to affect the universal nature of the dynamics. If a simplified vibrational Hamiltonian (effective or resonance Hamiltonian) is used, the choice of basis becomes more important if accurate dynamics are desired. For simplicity, we will discuss the dynamics in terms of a normal mode basis, which turns out to be a reasonable feature basis for $SCCl_2$.

An ideal feature basis would adapt to the structure of state space. For example, when two vibrational progressions tune through resonance due to anharmonicity, they may best be approximated by a normal mode basis below resonance, but by a local mode (or more exotic) basis above resonance. Classically, this would correspond to a coordinate system with adaptive local action coordinates. Because we consider only the bound part of the potential here, state space provides a conveniently simple picture; in the presence of reactive modes, an equivalent momentum-coordinate picture may prove useful in the future, and we expect a power law analogous to eq 1 to emerge in such a formulation. In section 4 we will discuss a well-defined "optimal" choice for the feature basis.

b. A Simple Formula for the Dimension of the IVR Manifold in State Space. Consider a feature $|0\rangle$ excited by a short laser pulse, shown in red in Figure 1. It is characterized by a set of quantum numbers $\mathbf{n}_0$. At short times it will evolve into a superposition

$$|\Delta t\rangle = e^{-(i/\hbar)\hat{H}\Delta t}|0\rangle \approx |0\rangle - i\frac{\Delta t}{\hbar}\hat{H}|0\rangle \qquad (2)$$

The amplitude that has leaked into another state $|i\rangle$ in state space is therefore

$$c_{i0} \approx i\frac{t}{\hbar}\langle i|H_{vib}|0\rangle = i\frac{t}{\hbar}V_{i0} \qquad (3)$$

The probability density distribution in state space is approximately given by

$$P_{i0} = |c_{i0}|^2 = |\frac{t}{\hbar}V_{i0}|^2 \qquad (4)$$

P_{i0} defines a manifold embedded in state space − a manifold of those states among which the IVR initiated in $|0\rangle$ occurs. Some states are efficiently coupled, such as by the Fermi resonance indicated in Figure 1b; others are not, and the flow of probability is therefore anisotropic.[15]

This manifold is the hypervolume in state space on which the wave packet initially moves, if we consider the quantum evolution as a diffusion-like process. The local dimension of the manifold about $\mathbf{n}_0$ is given by[22]

$$D_v = \frac{\partial \ln \Sigma P_{i0}}{\partial \ln n}\Big|_{\mathbf{n}_0} \quad D_v(n) = \frac{\Delta \ln \Sigma P_{i0}}{\Delta \ln n}\Big|_{\mathbf{n}_0} \qquad (5)$$

where $n = |\mathbf{n} - \mathbf{n}_0|$ is the distance from state $|0\rangle$ to state $|i\rangle$ and the sum over i is over all states $|i\rangle$ which satisfies $|\mathbf{n} - \mathbf{n}_0| \leq$ n. For example, if all couplings c_{i0} from $|0\rangle$ to the

surrounding states $|i\rangle$ were identical, and if the flow in the three-dimensional state space of Figure 1 were not restricted by energy conservation, then $\Sigma P_{i0} \sim n^3$ and $D_v = 3$, in accord with intuition. As another example, the manifold shown in Figure 1C is restricted to the energy shell and has a dimension $1 < D_v < 2$. If D_v were less than 1, only isolated patches of resonantly coupled states would exist in state space, and there would be no IVR.

In practice, the sum in eq 5 must be evaluated as a finite difference because the state space is discrete. Each state $|0\rangle$ is surrounded by shells of hyperpolyhedra with $n = 1, 2, 3, 4...$ (octahedra for $N = 3$), which may be truncated if the state lies near the edge of the state space or energy conservation is invoked.[13] The resulting $D_v(n)$ depends on the initial state and also on which pair of hyperpolyhedra is used to evaluate eq 5, as indicated on the right-hand side of the equation by the dependence of D_v on n.

Eq 4 does not impose the necessary restriction of the probability flow to the energy shell at long times. This restriction is a natural consequence of the full quantum dynamics following finite bandwidth laser excitation, but not accounted for by perturbation theory. In the full dynamics, a state far off the energy shell can only participate in the dynamics on a time scale satisfying

$$\Delta E_{i0} \Delta t \approx \hbar \tag{6}$$

Introducing this constraint into eq 4, one obtains

$$P_{i0} \approx \left(\frac{V_{i0}}{\Delta E_{i0}}\right)^2 \tag{7}$$

Finally, when $|\Delta E_{i0}| < |V_{i0}|$, $|0\rangle$ and $|i\rangle$ are strongly mixed. Such states $|i\rangle$ make the maximum possible contribution to the IVR flow manifold, and eq 7 should not increase further. It has been shown that the function

$$L_{i0}^2 = [1 + (\Delta E_{i0}/V_{i0})^2]^{-1} \tag{8}$$

provides a good description of the state mixing among pairs of states both in the perturbative and resonant limits,[6] and we will therefore use it instead of eq 7 to evaluate the dimensionality of the flow manifold, which is then given by

$$D_v(n) \approx \frac{\Delta \ln \Sigma L_{i0}^2}{\Delta \ln n}\Big|_{\mathbf{n}_0} \tag{9}$$

Equation 9 is an approximate formula for the dimensionality of the manifold on which the IVR wave packet originating in state $|0\rangle$ explores the state space. The dimension of this manifold generally lies between 1 and $N - 1$ or N, depending on the excitation conditions (the example in Figure 1c has $1 < D_v < 2$). For $D_v < 1$, there are only disconnected patches of resonantly interacting states, and IVR in the usual sense no longer occurs. If energy redistribution in state space is indeed a quantum diffusion process as given by eq 1, then D_v, which can be obtained without computing actual dynamics, should equal the power law coefficient δ obtained from $P(t)$ or from spectra (via eq 12 below).

c. Limitations of the Formula. A number of approximations were made in deriving eq 9, which will limit its applicability and are worth discussing in detail. However, eq 9 will be seen in sections 3 and 4 to yield very reasonable results compared to exact calculations of the exponent δ.

$D_v(n)$ depends on the initial state $|0\rangle$ and order of coupling n. However, eq 9 does not take into account averaging of D_v once multiple feature states are populated. At the very least, one should average over states coupled to $|0\rangle$ by different orders n. Our computational results (section 3b) indicate that regions of state space with very different values of D_v tend to be partitioned from one another. Simply evaluating at $\mathbf{n}_0$ is therefore a good approximation for the dimension of the IVR flow manifold originating from a given state $|0\rangle$, as long as one averages over all orders of coupling from that state.

If a pure normal mode basis is used, the nonresonant anharmonicity as well as changes in the optimal feature basis are neglected. Neglect of anharmonicity in evaluating ΔE_{i0} means that vibrational progressions cannot go into and out of resonance. In systems with large anharmonicities, one can partially correct for this by using an anharmonic feature basis which provides correct eigenvalues for edge states of the type $|0,\cdots n_i,\cdots,0\rangle$. Alternatively, one can replace H_{vib} by a contact-transformed effective Hamiltonian which explicitly separates resonant interactions from nonresonant interactions responsible for anharmonic constants such as χ_{ij}. Either approach allows the differences ΔE_{i0} to shift for different states $|0\rangle$ and $|i\rangle$ with the same $\Delta\mathbf{n} = \mathbf{n} - \mathbf{n}_0$. How one should transform the full vibrational Hamiltonian into the most appropriate effective Hamiltonian is an unresolved question in general. In section 3 we do present a simplified effective resonance Hamiltonian for $SCCl_2$ and later compare it with the full Hamiltonian matrix evaluated in a normal mode basis. In section 4, we develop a criterion for the "optimal" feature basis.

Equation 9 also neglects certain off-resonant couplings (superexchange).[23] As illustrated in Figure 1b, states far away from the energy shell can make significant contributions to the dynamics if they have sufficiently large coupling matrix elements. Equation 6 allows such states to participate only if they couple back directly to $|0\rangle$. This constraint therefore does not take off-resonant coupling chains into account properly. However, it has been shown that in most molecules direct and off-resonant chain contributions are of comparable importance at sufficiently high E and ρ_{tot};[13] their contributions to L_{i0}^2 generally lie within an order of magnitude of one another. Since eq 9 depends logarithmically on the couplings, D_v could be underestimated by as much as $\Delta D_v = 2$ if superexchange dominates the dynamics.

A completely rigorous proof of the correct value of the temporal exponent δ, to which eq 9 is an approximation, will require a nonperturbative approach to the probability flow, such as renormalization of the state space. Renormalization techniques have their own convergence problems,[24] and it is not clear at present whether such an approach would produce a formulation more accurate than eq 9.

3. Numerical Results

a. Potential Surface and Computational Methods. To test eq 9 in detail, we have chosen a recently developed potential surface for the tetratomic molecule $SCCl_2$.[3] An $N = 3$ system is too small because only the range $1 < D_v < 2$ can be covered using quasi-microcanonical preparation. At $N = 6$, $SCCl_2$ is large enough to allow nontrivial deviations of D_v from the minimal or maximal postulated dimensions (1 and 5). On the other hand, it is sufficiently small that one can perform full quantum dynamics simulations for comparison of the resulting $P(t)$ with eqs 1 and 9. A final reason for the choice is that $SCCl_2$ has only low-frequency vibrations. It is therefore a model for

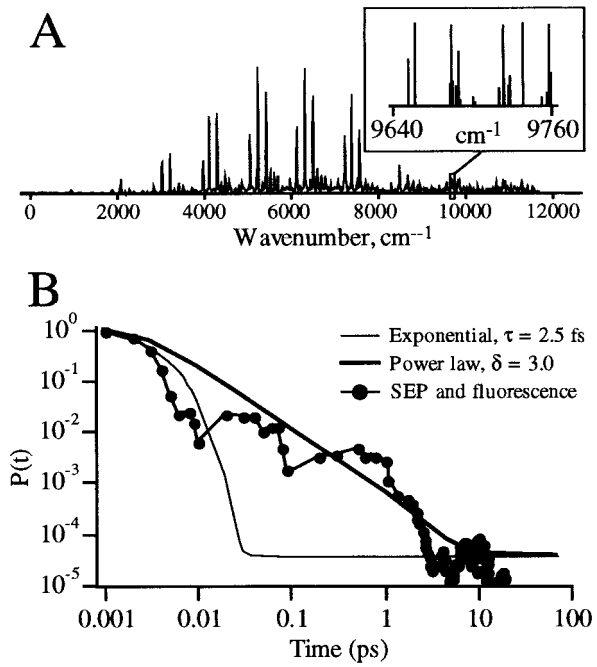

Figure 2. (A) Experimental fluorescence and SEP spectra of $SCCl_2$, the test system used in the calculations. The spectrum has a hierarchical structure in the 10 000 cm^{-1} to 0.1 cm^{-1} range. (B) $P(t)$ computed from the experimental spectrum, with a 10^5 dynamic range corresponding to the spectral coverage and resolution. The short time dynamics can be fitted by an exponential function, the overall dynamics by a power law with $\delta = 3$.

IVR among backbone modes, which dominate any IVR process at intermediate and long times.

The surface from ref 3 is a fourth order normal mode expansion derived by variationally fitting a curvilinear coordinate PES[12,25] pregenerated using ab initio calculations to about 100 IR, fluorescence and SEP transitions covering ground-state vibrational levels from about 300 to 10 000 cm^{-1}.[3] The root-mean-square accuracy of the predicted energy levels is about 5 cm^{-1}. The normal mode surface was obtained by directly computing numerical derivatives of the analytical surface.

For reference, the relevant experimental spectra are shown in Figure 2.[3] The spectrum has a highly hierarchical structure, proceeding from an overall envelope of 10 000 cm^{-1} width, to polyads $\approx$800 cm^{-1} width, to features of $\approx$100 cm^{-1} width, which contain clusters of $\approx$ <1−20 cm^{-1} in width made up of individual vibrational levels (inset). From this type of structure one would not expect an exponential decay. The survival probability $P(t)$ for excitation of the entire spectrum, computed directly from the fluorescence and SEP data, is also shown in Figure 2. It is seen to have the characteristic power law with superimposed quantum beats. The overall spectrum is well fitted by an exponent $\delta = 3.0$, and hence not well characterized by an exponential decay ($\delta = \infty$, see eq 13).

Many of the potential constants of the normal mode surface describing the spectrum in Figure 2 are rather small. As discussed in the previous section, such terms are expected to contribute mainly to nonresonant shifts of the vibrational energy levels. To create a simpler effective Hamiltonian which captures the most important interactions in the system, we combined a standard expansion in $(v_i + 1/2)$ with the most important resonance terms. The harmonic frequencies and anharmonic constants were estimated by direct fit to vibrational levels in several IR and fluorescence spectra.[3,26,27] The resonant terms were taken from the normal mode surface by generating all frequency combinations

$$\Delta\omega\{n_i\} = \sum_{i=1}^{6} n_i\omega_i \quad \sum_{i=1}^{6}|n_i| \le 4 \tag{10}$$

and selecting only potential constants $V\{n_i\}$ such that $R = |V\{n_i\}/\Delta\omega\{n_i\}| > 0.05$. The resulting approximate resonance Hamiltonian has the form

$$H_{eff} = \sum_i \omega_i(v_i + 1/2) + \sum_{i,j}\chi_{ij}(v_i + 1/2)(v_j + 1/2) + \sum_{\{n_i\}} V_{\{n_i\}}\prod_i (a_i^\dagger + a_i)^{n_i} \tag{11}$$

with constants summarized in Table 1. Only six resonance terms exceed the criterion $R > 0.05$. It should be noted that the resonance criterion R is smaller than 0.05 for all couplings involving modes 4 (out of plane bend) and 3 (symmetric bend). The largest symmetry-allowed couplings involving these two modes are also shown in Table 1. Because of the nature of the potential constants in Table 1, none of the interactions in the second line of eq 11 make contributions to the diagonal energy; otherwise, such contributions would have to be projected out of the summation.

Both time-dependent and time-independent calculations were carried out to study the vibrational dynamics of the system. For time-dependent calculations, the SUR symplectic propagator was used.[28,29] The initial states $|t=0\rangle$ were chosen from a normal mode basis, including both interior and edge states (see b. below).[10] The vibrational numbering is the same as that used in ref 3 (ν_1 CS stretch, ν_2 A_1 CCl stretch, ν_3 A_1 bend, ν_4 out of plane bend, ν_5 B_2 CCl stretch, ν_6 B_2 bend). Wave packets were factored into vibrational symmetry blocks to speed up the calculation. Convergence was tested as a function of energy window size and a perturbative state filter criterion L similar to eq 8 (e.g., a >4000 cm^{-1} window and $L \approx 0.01$ converged the $|233222\rangle$ interior state near 7922 cm^{-1}). The output of the calculation yielded the complex time-dependent expansion coefficients $c_{0i}(t)$ of the wave packet in the normal mode basis.

Some of the smaller calculations were checked using the matrix-fluctuation−dissipation theorem[30,31] in combination with Lanczos matrix diagonalization[32,33] to obtain spectral intensities without calculation of the eigenfunctions. Again, convergence was tested as a function of window size and L; the convergence criteria were found to be similar to the corresponding time-dependent calculations. Windowing effects were also investigated by generating Lorentzian line shapes with widths corresponding to $P(\tau) = 1/e$, truncated to the window size used in the calculations. The resulting $P(t)$ could be fitted by exponential decays with superimposed slight oscillations; no power laws were required.

b. IVR Dynamics. The survival probability $P(t)$ is a particularly simple measure of the IVR process and can be computed from time domain data or frequency domain data as

$$P(t) = |\langle 0|t\rangle|^2 = \sum_i I_i^2 + 2\sum_{j>i} I_i I_j \cos[\omega_{ij}t] \tag{12}$$

At long times, the survival probability oscillates about the small "dilution factor" $\sigma = \Sigma I_i^2$, which is the inverse of the number N_p of states participating in the IVR process.[34,35] Here, σ was determined from the asymptotic value of $P(t)$. Decays computed on the full surface for several states in the $E \approx$ 7000−9000

TABLE 1: Parameters for the Simplified Resonance Hamiltonian of $SCCl_2$[a]

$\omega_1 = 1149$	$\chi_{11} = -4.3$	$\chi_{12} = -2.5$		$\chi_{14} = -3.8$
$\omega_2 = 508$			$\chi_{23} = 2.0$	$\chi_{24} = -4.0$
$\omega_3 = 291$			$\chi_{33} = 1.0$	$\chi_{34} = 0.1$
$\omega_4 = 476$				$\chi_{44} = -0.2$
$\omega_5 = 806$				
$\omega_6 = 303$				

$V\{n_i\}$	n_{tot}	mode number n_i						resonance condition						R
		1	2	3	4	5	6	1	2	3	4	5	6	
−11.5	3	0	1	0	0	1	1	0	−1	0	0	1	−1	1
−5.4	4	1	1	0	0	2	0	−1	−1	0	0	2	0	0.22
34.5	3	1	0	0	0	2	0	1	0	0	0	−2	0	0.07
4.9	3	0	1	0	0	0	2	0	1	0	0	0	−2	0.06
7.9	3	1	2	0	0	0	0	1	−2	0	0	0	0	0.06
−31	3	0	1	0	0	2	0	0	−1	0	0	0	0	0.06
−7.7	3	0	0	1	0	1	1	0	0	−1	0	1	−1	0.04
9.8	3	0	1	0	2	0	0	0	1	0	−2	0	0	0.02

[a] Only coupling constants V satisfying $R = |V/\Delta\omega| > 0.05$ are shown, except for those involving modes 4 and 6, where the largest coupling constants have been included. The vibrational numbering follows the Mulliken symmetry convention.

cm^{-1} range are shown in Figure 3. They can be fitted to a power law of the form

$$P(t) = (1 - \sigma)\left(1 + \frac{2t}{\delta\tau}\right)^{-\delta/2} + \sigma \qquad (13)$$

or similar equations which describe the early-time rolloff.[17] Equation 13 has the advantage that it approaches an exponential as $\delta \rightarrow \infty$, allowing unbiased comparison with an exponential decay at long times. The exponents δ derived from the fits are tabulated for various initial states in Table 2. It should be noted that at present we have no theory which connects the initial cos−rolloff/exponential regions with the intermediate time regime in a rigorous manner. While fitting models alternative to eq 13 have little effect in those cases where σ is small and δ is large, they do introduce additional uncertainties into the exponents for the edge states in Figure 3 and Table 2.

The edge states (those with most quanta equal to zero, and hence at the edge of the state space in Figure 1) are seen to have smaller powers than energetically nearby interior states of state space. In fact, δ lies near the localization threshold of 1, where the IVR manifold breaks up into disconnected patches in state space. Correspondingly, the dilution factors in Figure 3 and Table 2 are relatively large. This is expected for a compact molecule in which vibrational modes cannot become highly localized: edge states have fewer neighbors to couple to, hence undergo IVR more slowly. It should be noted that the opposite was first observed experimentally and interpreted correctly in "extreme motion states" of 1-propyne.[36] In a larger molecule, particularly in a chain molecule, vibrational modes tend to be more localized. The energy of an interior state is then broken into smaller, approximately isolated packets, which behave more harmonically and undergo slower IVR.[13]

The fact that nearly degenerate edge and interior states can have such different IVR decays is a clear indication that the local coupled density of states, not the total density of states, controls IVR dynamics. The local number of coupled states in Table 2 (computed as in ref 37) correlates well with δ and σ; the total density of states does not. A large range of δ and σ is also observed for the resonance Hamiltonian (see below), with slower and less complete IVR for states nearer the edge of state space. The difference in dilution factors indicates large variations in fragmentation for nearly isoenergetic bright states, with some states approaching the statistical value of σ, while others have σ near unity. Similar fluctuations among overtones or combination states have been observed experimentally in $SCCl_2$ (Figure 2 inset),[3] as well as in other organic molecules.[34,38]

Figure 4 shows the average harmonic vibrational occupancies for the $|700000\rangle$ and nearby $|233222\rangle$ initial states. They were evaluated by expanding the IVR wave packet $|t\rangle = \Sigma c_{i0}|i\rangle$ in terms of harmonic feature states $|i\rangle = |n_1 \cdots n_6\rangle$ and calculating the expectation values $\langle v_i\rangle = \langle t|a_i^\dagger a_i|t\rangle$. The edge state undergoes very little decay in the v_1 quantum number. It is only weakly coupled to the surrounding bath states. In contrast, the nearby interior state rapidly reaches a set of equilibrated $\langle v_i\rangle$, which are close to those predicted by the Bose−Einstein distribution for the energy $E \approx 7920$ cm^{-1} of the $|233222\rangle$ state and the frequencies listed in Table 1. In effect, the $|233222\rangle$ state rapidly mimics a thermalized system, inasmuch as a 6-D system can do that. In this context, it is interesting to note that the molecule appears thermalized in the *full* 6-D vibrational manifold. This is so even though δ is less than 3, implying an IVR manifold which cannot completely cover the state space since it is of smaller dimension. Classically, the dimensionality argument holds rigorously; quantum mechanically, the finite size of the state volume $\approx h^n$ makes this argument less convincing. When the fractal dimension $D_v < N - 1$, the IVR manifold can nonetheless be embedded in state space in a highly folded manner which gives the impression of thermalization for a highly averaged variable such as $\langle v_i(t)\rangle$. It would be interesting to study how deeply the coherence of even such a small system must be probed before its fundamentally nonthermal pure state nature reemerges.

For comparison, Figure 5 shows the $P(t)$ obtained by propagating the $|233222\rangle$ initial state with the effective Hamiltonian of Table 1. Although the survival probability is generally slightly larger than observed with the full Hamiltonian, δ is very similar, and the qualitative nature of the dynamics is well described by the resonance Hamiltonian.

It is evident from Figures 3 and 5 that, in addition to the average decay discussed here, $P(t)$ is subject to quantum beats with rms amplitude $B(t)$. For a large system, $B(t)/P(t)$ is initially negligibly small; at long times, $\bar{B}(t)/\bar{P}(t) = \bar{B}(t)/\sigma \approx 1$:[35] fluctuations of the populations in state space, albeit small on an absolute scale (mini-quantum beats), become pronounced compared to the populations $|c_{i0}|^2$ themselves. At intermediate times, the mini-quantum beats give additional clues to the mechanism of energy transport. Although in this paper we fit only the average behavior, one observation illustrated by Figure 5 is worth making: Invariably, the mini-quantum beats com-

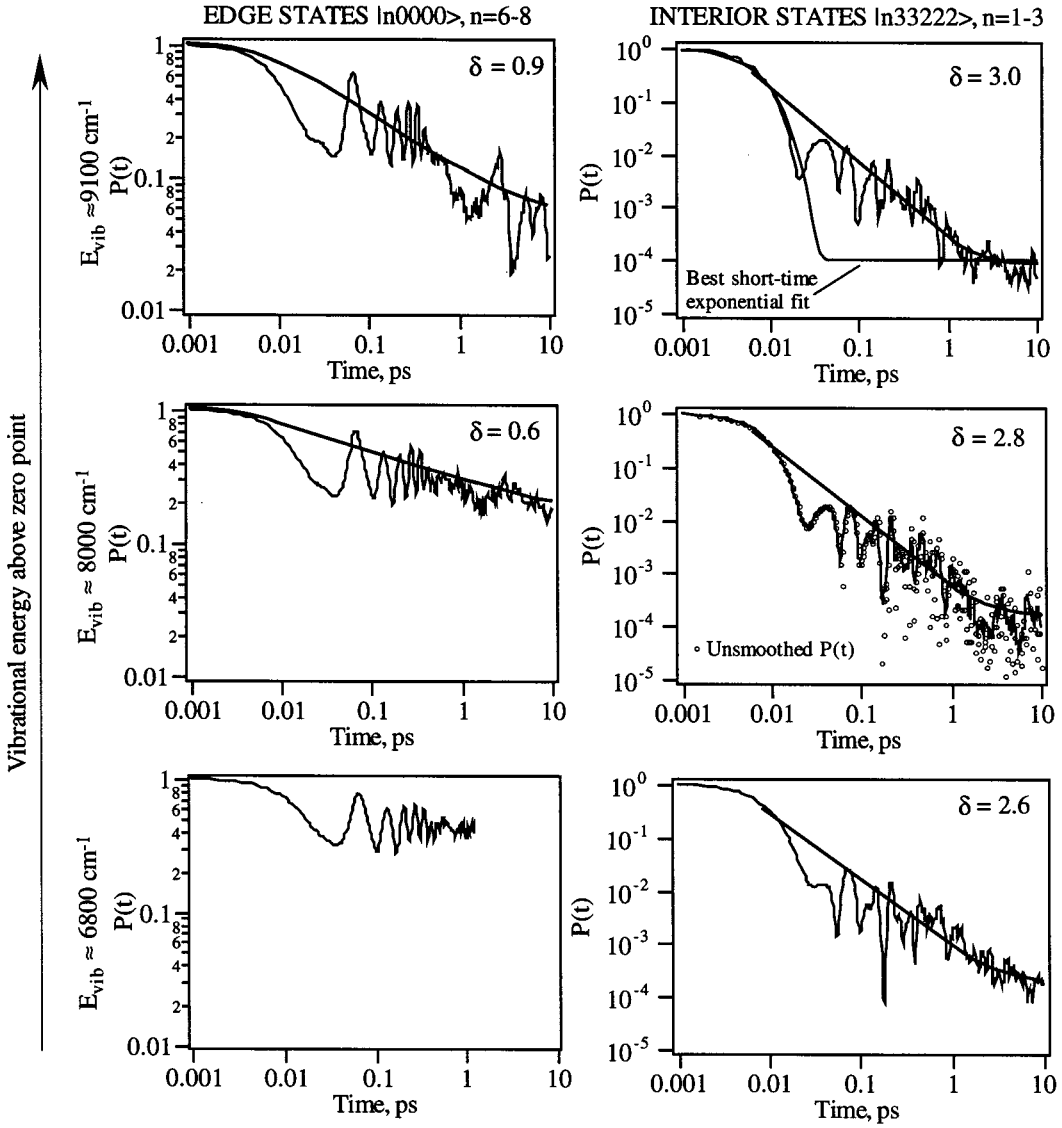

Figure 3. IVR decays of representative edge and interior states sampling three energy ranges. SUR calculations were 5-point smoothed to reduce the mini-quantum beat amplitude and show the average behavior; for the $|233222\rangle$ state (right center), the circles illustrate the fluctuations of the unsmoothed $P(t)$. For the interior states, eq 13 is plotted in black. For the edge states with $n = 7$ and 8, $P(t)$ was fitted to the equation in ref 17, which accounts for the correct rolloff at $t = 0$; no reliable estimate of δ was possible for the $n = 6$ case. The second curve for the $|333222\rangle$ state (right top) shows the best-fit exponential (weights inversely proportional to weight all time scales equally on a log−log plot) for comparison.

TABLE 2: Comparison of Power Law Coefficients from Experiment, Quantum Dynamics Using the Full Vibrational Hamiltonian (Δ), and Eq 9 (D_v)

state	E_{bright}	$\bar{D}_v$[b]	δ	σ	N_{loc}[c]	ρ_{tot}[d]
experiment[a]						
full spectrum			2.8			
H_{vib}						
$\|600000\rangle$	6905			0.4	0.3	5.8
$\|133222\rangle$	6771	2.5(2)	2.6(1)	0.0003	4.8	5.5
$\|700000\rangle$	8055	0.6(2)	0.6(3)	0.1	0.4	10.4
$\|233222\rangle$	7922	2.7(2)	2.8(1)	0.0001	8.5	9.9
$\|800000\rangle$	9206	0.7(2)	0.9(3)	0.02	0.5	18.1
$\|333222\rangle$	9072	2.8(2)	3.0(1)	9×0^{-5}	12.6	17.2

[a] SEP and fluorescence following $1_0^2\tilde{B}$ excitation. [b] Average of $D_v(3)$ evaluated using $n = 1$ and 3, and $D_v(4)$ evaluated using $n = 2$ and 4, corresponding to the cubic and quartic terms in H_{vib}. [c] The local number of coupled states was evaluated as discussed in ref 38. [d] In cm^{-1}; evaluated in a 50 cm^{-1} window surrounding the bright state.

puted for H_{res} are smaller than those obtained for the full Hamiltonian H_{vib}, although the average $\bar{P}(t)$ are similar; couplings weaker than those included in our minimal resonance Hamiltonian, and a fuller accouting for anharmonicity, are necessary for the mini-quantum beats.

$P(t)$ and its parameters σ, δ, and τ are not alone an adequate description of the dynamics because they focus mainly on the history of the initial feature or "bright" state. At the very least, one would also like to know how the rest of the vibrational wave packet is dispersing through state space.[39] For example, the probability could be hopping to many energetically accessible dark states at once. In that case, the component of the wave packet orthogonal to $|0\rangle$ is highly dephased from the outset. Or the probability could be hopping to only a few additional features. In that case, the energy flow has the hierarchical structure often described as a "tier picture". Figure 6 illustrates for the $|700000\rangle$ and $|333222\rangle$ states how the IVR wave packet disperses in state space. Figure 6A,B shows the dispersion in three linearly independent combinations of vibrational quantum numbers based on the effective Hamiltonian in Table 1, while Figure 6C shows the gradual dispersion as a function of time and energy, corresponding to a tier structure.

Figure 6C shows that the probability disperses gradually into other feature states. Although no tiers were imposed a priori

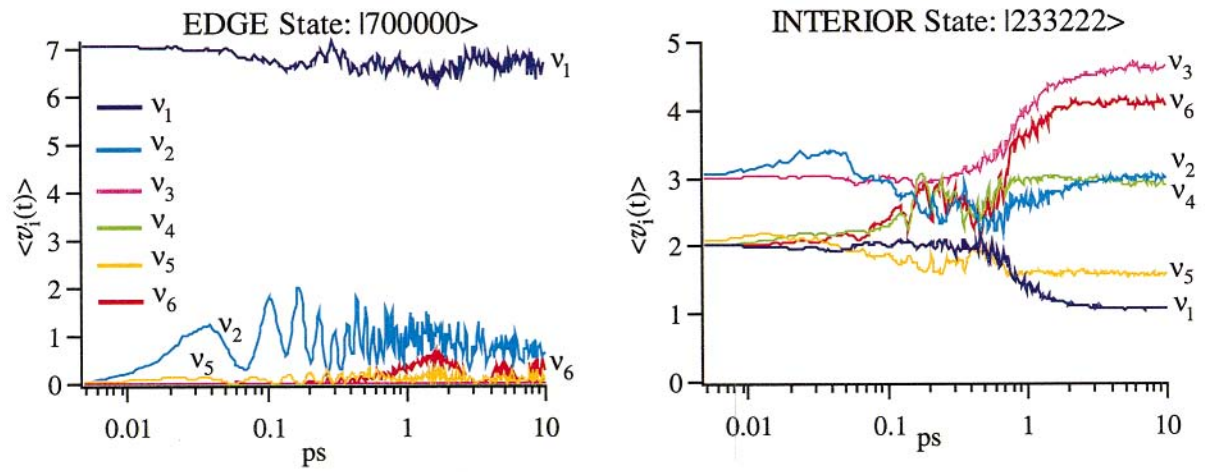

Figure 4. Average vibrational quantum distributions as a function of time for an edge and interior state. The edge state with D_v and $\delta \approx 0.8$ lies below the IVR threshold and shows resonant behavior without complete energy flow. On the other hand, the interior state $\langle v_i \rangle$ values rapidly equilibrate to those expected from Bose−Einstein statistics, with populations sorted by the vibrational frequency. Such a state can be said to have reached a "thermal equilibrium" within the bath of vibrational modes. In both cases, the ν_3 and ν_4 modes are particularly slow at taking up population or reaching equilibrium.

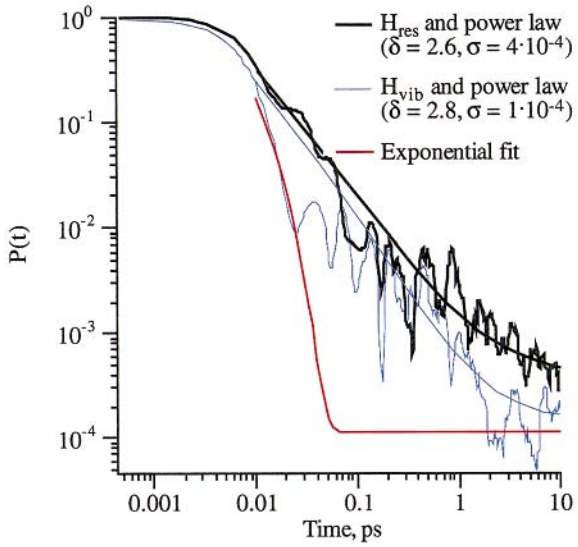

Figure 5. SUR calculation for the |233222⟩ bright state using the effective resonance Hamiltonian of eq 11. For comparison, the $P(t)$ from the full Hamiltonian is shown; both are fitted by very similar power law exponents. An exponential with constant weighting (to fit the short-time data) is also shown, and greatly underestimates $P(t)$ after about 0.01 ps.

on the calculation, one can therefore assign tiers to the energy flow, as discussed previously.[10] Contrast this to a "Golden Rule" basis, composed of the feature state $|0\rangle$, and the eigenstates of $H_d = QH_{vib}Q$, where $Q = I - |0\rangle\langle 0|$. In a Golden Rule basis, the dispersing wave packet samples all bath states simultaneously (although in a correlated manner as described below). This is so because the bath states are already highly premixed and dephased. Although the exact dynamics are equally well obtained in a Golden Rule basis, first-order time-dependent perturbation theory applied to such a basis and leading to Fermi's Golden Rule is sufficient only at short times: if U_d is the operator diagonalizing H_d, then the actual off-diagonal matrix elements in the Golden Rule matrix are given by

$$\hat{V}^{GR} = U_d^{\dagger}\{PH_{vib}Q + QH_{vib}P\}U_d \qquad (14)$$

These matrix elements are highly correlated with one another because of the hierarchical structure of the vibrational Hamiltonian exposed by Figure 6 and cannot be represented by uncorrelated random couplings V_{i0}^{GR}, as is usually done in the application of the Golden Rule. As a result, the power laws in Figures 2 and 3 arise instead of exponential dynamics.

4. Discussion

Table 2 shows the values of $\bar{D}_v$ calculated from eq 9. $\bar{D}_v$ is the average of $D_v(3)$ and $D_v(4)$, weighted by the local density of states coupled by cubic and quartic terms, respectively. We find that the manifold of cubic couplings generally has a lower dimension than the manifold of quartic couplings. The agreement between the dynamical observable δ and the IVR manifold dimension $\bar{D}_v$ is very good for all states in Table 2. In particular, edge states have small values of $\bar{D}_v$ and δ, while interior states have larger values. A quantum diffusion picture for the IVR process is therefore appropriate, and eq 9 provides a satisfactory expression for the dimension of the IVR manifold embedded in state space, at least for the examples studied here. The fact that this number can be calculated using only short-time evolution (eq 3) in a feature basis indicates that the dynamics are controlled by the local structure of state space. Moreover, the fact that a feature state space is sufficient indicates that the vibrational Hamiltonian, even at substantial total energy E, retains a memory of the simple effective Hamiltonian (e.g., eq 11) which provides a zero-order approximation at low energies. It has been discussed elsewhere that this is due to the small value of the Born−Oppenheimer parameter $\kappa = \sqrt{(m_e/m_P)}$, which is responsible for the large ratio of the electronic:vibrational:anharmonic:rotational energy scales of molecules.[7,10,11,17,40]

The good agreement indicates that for $SCCl_2$ superexchange coupling chains are at most comparable to direct couplings. This is not surprising in a compact molecule with many low-frequency vibrations. In a larger system with XH stretching or bending modes, one would expect corrections due to superexchange to appear. As described in section 2, one can realistically expect this underestimate to be as large as $\Delta D_v = 2$. However, the qualitative picture remains unchanged, and for backbone vibrations involving low frequency motions, which are most interesting from the point of view of controlling chemical reactivity, the error is likely to be <2 in most cases.

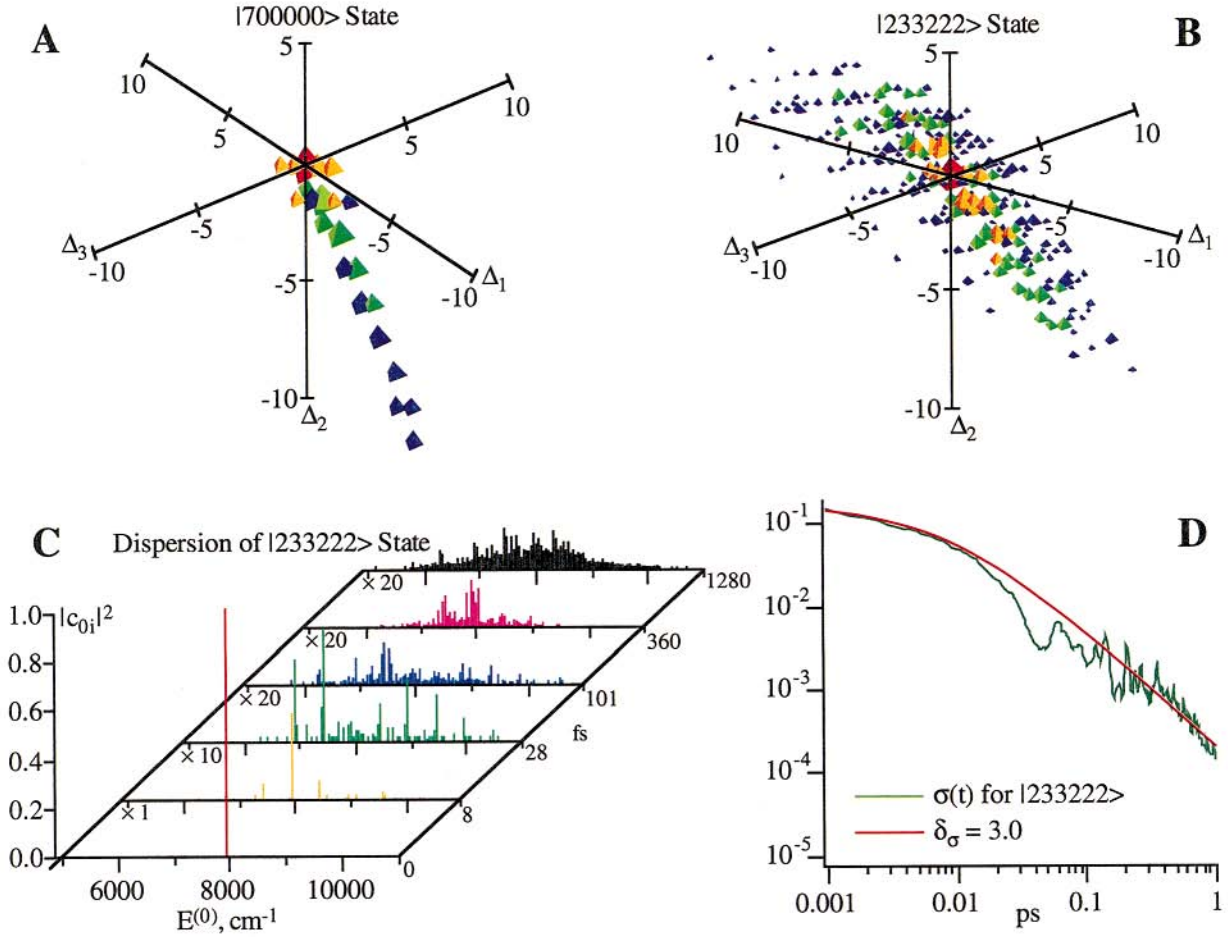

Figure 6. Dispersion of the IVR wave packet in state space. The axes in A and B are labeled in terms of the most important resonances in Table 2: $\Delta_1 = (0, -1, 0, 0, 1, -1)$, $\Delta_2 = (-1, -1, 0, 0, 2, 0)$, and $\Delta_3 = (1, 0, 0, 0, -2, 0)$; the color code corresponds to the 0, 8, 28, and 101 fs times in C; the size of each point is $\ln|c_{i0}|^2$. (A) Edge state: the probability flow is an at most 1-dimensional "jet" in the Δ_1/Δ_2 plane. (B) Interior state: the probability flows into a three-dimensional manifold, but it is still anisotropically flattened in the Δ_3 direction, corresponding to the smaller L for that resonance in Table 1. (C) Dispersion of an interior state with $|c_{i0}|^2$ of all participating features shown; new feature states appear gradually. (D) $\sigma(t)$ for C, showing that the number of features participating in the dynamics indeed grows as a power law only. The power δ_σ is the same as that observed for the corresponding $P(t)$ in Figure 3.

The experiment in Figure 2, as well as the wave packet propagation and analytical formula, all yield a dimensionality near 3 for interior and partially interior states, and less for edge states. Both are considerably less than the maximum possible value of 5−6. The edge states are easily explained in terms of the smaller number of coupling partners. The $|n00000\rangle$ states in particular diffuse mostly along one single resonance direction in state space: Figure 6A shows a "probability jet" in state space emanating from the initially prepared $|700000\rangle$, which fans out only slightly, accounting for the low dimension $\bar{D}_v \approx 0.8$ (1.0 in the full dynamics calculation used to plot Figure 6A).

The interior states can be rationalized in terms of the effective Hamiltonian in eq 11. Table 1 shows that the six largest interactions do not involve the ν_3 (symmetric bending) and ν_4 (out of plane bending) modes at all. They only contribute with a resonance criterion $R \leq 0.03$. One would therefore expect the vibrational energy flow to be facile among all modes except 3 and 4. To a first approximation, the IVR manifold is subject to the condition $\Delta v_3 = \Delta v_4 = 0$, introducing approximately good quantum numbers. With the addition of energy conservation (within the bandwidth), the resonance Hamiltonian therefore yields $D_v \approx 6 - 2 - 1 = 3$, close to the experimental and computed values. Figure 6B shows the evolution of the $|233222\rangle$ state (nearly isoenergetic with $|700000\rangle$) in the subset of state space comprising the three strongest resonances in Table 1. Although the expansion of the evolving IVR wave packet throughout state space is more uniform (in keeping with $D_v \approx 3$), even here structure due to the different strength of the resonances (R in Table 1) is evident. In the full state space, plot 6B would appear as an expanding disk which initially remains thin in the Δv_3 and Δv_4 directions. That ν_3 and ν_4 contribute only on a long time scale is also evident from Figure 4: energy flow from the $|700000\rangle$ state is slow, but the increase in $\langle v_3 \rangle$ and $\langle v_4 \rangle$ is particularly slow, and they are last to reach equilibrium starting with $|233222\rangle$.

It is realistic to expect that D_v remains fairly small even in large molecules: this has already been deduced from several experiments and quantum dynamics calculations.[17] The reason for this expectation is straightforward: although a large molecule has more nearly degenerate and low-frequency modes which could in principle become resonant, these modes tend to be localized. Mixed potential constants (such as the ones for $SCCl_2$ in Table 1) are mostly very small. This has also been found in statistical analyses of potential constant distributions. (It is not true for liquids, clusters or macromolecules with a highly corrugated energy landscape, to which this analysis does not apply.[12,13]) If this is true, then much can be learned about the IVR mechanism and value of D_v in large molecules by studying reduced dimensionality resonance Hamiltonians. So far, these

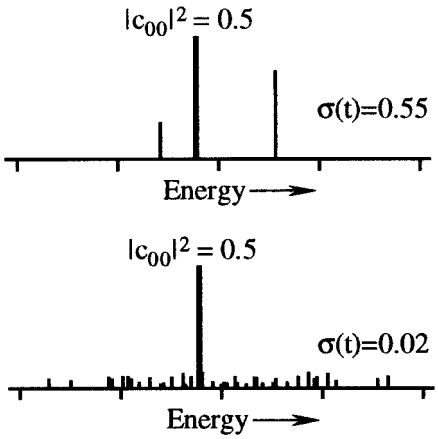

Figure 7. Two extreme cases of how amplitude flows from the initial state into other states such that $P(t) = 0.5$. In A, only a small number of states become active; in B, the same $P(t)$ is obtained but many more states have become active. The upper scenario corresponds to a properly selected feature basis; the lower scenario corresponds to an eigenstate or Golden Rule basis. The dispersion $D = \sigma(t)^{-1}$ can distinguish between the two cases.

have been applied mainly to small systems.[21] A general method for finding an appropriate resonance Hamiltonian which optimally tracks the IVR manifold embedded in the full dimensional state space would have to be developed.

The power law decays in Figure 3 illustrate the slowness of the IVR dynamics. As shown in Figure 6C, the IVR wave packet not only leaks slowly out of state $|0\rangle$, it also disperses slowly in state space. This behavior cannot be adequately captured by $P(t)$ alone, or by its associated parameters δ, τ, and σ. Figure 7 illustrates two extreme cases: $P(t) = |c_{00}|^2$ has decreased to 1/2 in both cases, yet in one case the wave packet has dispersed in state space far more extensively than in the other.

To remedy this we introduce a dispersion parameter $D = \sigma(t)^{-1}$ closely related to $\sigma^{-1} = N_p$, but applicable to the time-evolving IVR wave packet:

$$D = \sigma(t)^{-1} = \frac{(1-|c_{00}|^2)^2}{\sum_{i\neq 0}|c_{0i}|^4} + 1 \qquad (15)$$

where the $c_i = \langle i|t\rangle$ are again the expansion coefficients of the wave packet in the feature state basis $\{|i\rangle\}$. Just as N_p measures the number of participating eigenstates in a fragmented IVR spectrum, D measures the number of participating feature states excluding the initial bright state. (Hence the removal of c_0 from the normalization and the sum in the denominator.) For a molecule with substantial fragmentation, $\sigma(t)$ approaches the dilution factor σ as $t\rightarrow\infty$.

Figure 6D shows a plot of $\sigma(t)$ for dynamics initiated in the $|233222\rangle$ state. It can be seen that $\sigma(t)$ decays as a power law, just like the survival probability $P(t)$; hence the dispersion D increases very slowly in a feature basis. This is a nontrivial consequence of the structure of the molecular vibrational Hamiltonian H_{vib}. One can of course easily find bases in which D is large at all times $t > 0$. Examples are the eigenstates, or the "Golden Rule" basis discussed in the previous section. The converse is not true: not every Hamiltonian has a feature basis such that D is small over any significant time period. For example, a GOE Hamiltonian has no basis for which D is small, unless the initial state is an eigenstate: the couplings are unstructured and access most basis states immediately, in any representation.

The vibrational Hamiltonian therefore imposes a structure on state space which is well represented by feature basis sets, in the sense that they can describe the dynamics for the longest possible time with the smallest number of functions. In section 2a, it was stated that the exact choice of feature basis is irrelevant if one computes exact dynamics, but becomes relevant if one attempts a simplified description of the molecule. In light of eq 15, we can now make a reasonable definition of the optimal feature basis for IVR dynamics initiated in a state $|0\rangle$.

The optimal feature basis is the orthonormal set of functions $\{|i\rangle\}$ which includes $|0\rangle$ and maximizes

$$\lim_{t\rightarrow\infty} \int_0^t dt'\, \sigma(t') \qquad (16)$$

Equation 16 ensures that a minimum number of states will describe the IVR dynamics for as long as possible.

5. Conclusions

During IVR, the survival probability of the initially prepared state decreases toward the statistical limit via a slow power law process. The power δ can now be estimated from the vibrational potential constants using a simple formula. In addition, the IVR wave packet disperses only slowly throughout state space, unlike the wave packets governed by a random Hamiltonian, such as a GOE matrix. The classical tier picture of IVR therefore remains approximately valid to long times.

This has important consequences for the possibility of controlling IVR via manipulation of coherence. Feature states have a simple structure and should therefore be amenable to coherent control. For each such state, generally a complex amplitude (population and phase) has to be controlled, resulting in two control parameters. If the number of controllable feature states grows with time as $D(t)$, then the control problem up to time t requires $2D(t)$ parameters. The results of this work indicate that this number is not much larger than $P(t)^{-1}$, even if low-frequency backbone motions are involved in the IVR process. Experiments and calculations for larger organic molecules have already shown that $P(t)$ decays with a small power law coefficient. If $D(t)$ is only slightly larger than $P(t)^{-1}$ in those cases also, this opens the possibility for coherent manipulation of vibrational energy flow in larger molecules with a modest number of control parameters up to significantly long times. Here, $2D(t)$ is a much more useful upper bound than that provided by a Golden Rule or eigenstate picture without correlations, in which the guaranteed bound is an often unfavorable σ^{-1}.

Acknowledgment. The present work was supported by a grant from the National Science Foundation (CHE-9457970, and a Packard Fellowship. M.G. was a Sloan Fellow, Cottrell Scholar and Dreyfus Teacher−Scholar while this work was carried out. M.G. thanks the participants of the 1998 Telluride Summer workshop on Control and IVR for enlightening discussions, which crystallized much of the science discussed in this paper. Among these was Kent Wilson, a gentleman and scholar in the field of control and coherence, to whom this paper is dedicated.

References and Notes

(1) Solina, S. A. B.; O'Brien, J. P.; Field, R. W.; Polik, W. F. *J. Phys. Chem.* **1996**, *100*, 7797.

(2) Gambogi, J. E.; Kerstel, E. R. T.; Lehmann, K. K.; Scoles, G. *J. Chem. Phys.* **1993**, *100*, 2612.

(3) Bigwood, R.; Milam, B.; Gruebele, M. *Chem. Phys. Lett.* **1998**, *287*, 333.

(4) Boyarkin, O. V.; Lubich, L.; Settle, R. D. F.; Perry, D. S.; Rizzo, T. R. *J. Chem. Phys.* **1997**, *107*, 8409.
(5) Svitak, J.; Li, Z.; Rose, J.; Kellman, M. E. *J. Chem. Phys.* **1995**, *102*, 4340.
(6) Gruebele, M.; Bigwood, R. *Int. Rev. Phys. Chem.* **1998**, *17*, 91.
(7) Oka, T. *J. Chem. Phys.* **1967**, *47*, 5410.
(8) Rashev, S. *Chem. Phys.* **1990**, *147*, 221.
(9) Bullock, W. J.; Adams, D. K.; Lawrance, W. D. *J. Chem. Phys.* **1990**, *93*, 3085.
(10) Bigwood, R.; Gruebele, M. *Chem. Phys. Lett.* **1995**, *235*, 604.
(11) Gruebele, M. *J. Phys. Chem.* **1996**, *100*, 12183.
(12) Madsen, D.; Pearman, R.; Gruebele, M. *J. Chem. Phys.* **1997**, *106*, 5874.
(13) Pearman, R.; Gruebele, M. *J. Chem. Phys.* **1998**, *108*, 6561.
(14) Schofield, S. A.; Wolynes, P. G. *J. Chem. Phys.* **1993**, *98*, 1123.
(15) Schofield, S. A.; Wolynes, P. G. *J. Phys. Chem.* **1995**, *99*, 2753.
(16) Blumen, A.; Klafter, J.; Zumofen, G. *J. Phys. A* **1986**, *19*, L77.
(17) Gruebele, M. *Proc. Natl. Acad. Sci. U.S.A.* **1998**, *95*, 5965.
(18) Ezra, G. S.; Martens, C. C.; Fried, L. E. *J. Phys. Chem.* **1987**, *91*, 3721.
(19) Martens, C. C. *J. Stat. Phys.* **1992**, *68*, 207.
(20) Nesbitt, D. J.; Field, R. W. *J. Phys. Chem.* **1996**, *100*, 12735.
(21) Rose, J. P.; Kellman, M. E. *J. Chem. Phys.* **1996**, *105*, 7348.
(22) Mandelbrot, B. B. *The fractal geometry of nature*, 3rd ed.; W. H. Freeman: San Francisco, 1983.
(23) Mehta, A.; Stuchebrukhov, A. A.; Marcus, R. A. *J. Phys. Chem.* **1995**, *99*, 2677.
(24) Binney, J. J.; Dowrick, N. J.; Fisher, A. J.; Newman, M. E. J. *The theory of critical phenomena*; Clarendon Press: Oxford, 1992.
(25) Sibert, E. L. *Int. Rev. Phys. Chem.* **1990**, *9*, 1.
(26) Brand, J. C. D.; Hardwick, J. L.; Teo, K.-E. *J. Mol. Spectrosc.* **1975**, *57*, 215.
(27) *Gmelin's Handbuch der anorganischen Chemie, achte Auflage vol.* ***CD6***; Springer: Berlin, 1983.
(28) Bigwood, R.; Gruebele, M. *Chem. Phys. Lett.* **1995**, *233*, 383.
(29) Gray, S. K.; Verosky, J. M. *J. Chem. Phys.* **1994**, *100*, 5011.
(30) Gruebele, M. *J. Phys. Chem.* **1996**, *100*, 12178.
(31) Gruebele, M. *J. Chem. Phys.* **1996**, *104*, 2453.
(32) Wyatt, R. E. *Adv. Chem. Phys.* **1989**, *73*, 231.
(33) Maynard, A. T.; Wyatt, R. E. *J. Chem. Phys.* **1995**, *103*, 8372.
(34) Stewart, G. M.; McDonald, J. D. *J. Chem. Phys.* **1983**, *78*, 3907.
(35) Pechukas, P. *Chem. Phys. Lett.* **1982**, *86*, 553.
(36) Gambogi, J. E.; Timmermans, J. H.; Lehmann, K. K.; Scoles, G. *J. Chem. Phys.* **1993**, *99*, 9314.
(37) Bigwood, R.; Gruebele, M.; Leitner, D. M.; Wolynes, P. G. *Proc. Natl. Acad. Sci. U.S.A.* **1998**, *95*, 5960.
(38) Yao, G.; Wyatt, R. E. *J. Chem. Phys.* **1994**, *101*, 1904.
(39) McWhorter, D. A.; Hudspeth, E.; Pate, B. H. *J. Chem. Phys.* **1999**, *110*, 2000.
(40) Rashev, S.; Nedev, N. *J. Mol. Struct.* **1992**, *266*, 247.